Acta Montanistica Slovaca
ISSN 1335-1788
actamont.tuke.sk

Dangerous Planar Rockfall in an Open Pit: A Case Study from Host'ovce Quarry, Slovakia

Jaroslav BUŠA[1], Julián KONDELA[2], Roman FARKAŠOVSKÝ[3] and Stanislav JACKO[4]*

Authors' affiliations and addresses:
[1] Institute of Geosciences, Faculty of Mining, Ecology, Process Control and Geotechnology, Technical University Kosice, Košice, Slovakia
e-mail: jaroslav.busa@tuke.sk

[2] Institute of Geosciences, Faculty of Mining, Ecology, Process Control and Geotechnology, Technical University Kosice, Košice, Slovakia
e-mail: julian.kondela@tuke.sk

[3] Institute of Geosciences, Faculty of Mining, Ecology, Process Control and Geotechnology, Technical University Kosice, Košice, Slovakia
e-mail: roman.farkasovsky@tuke.sk

[4] Institute of Geosciences, Faculty of Mining, Ecology, Process Control and Geotechnology, Technical University Kosice, Košice, Slovakia
e-mail: stanislav.jacko@tuke.sk

***Correspondence:**
Jaroslav Buša, Institute of Geosciences, Faculty of Mining, Ecology, Process Control and Geotechnology, Technical University Kosice, Košice, Slovakia
tel.: 0556023130
e-mail: jaroslav.busa@tuke.sk

Funding information:
This work was supported by the Scientific Grant Agency of the Ministry of Education, Research, Development and Youth of the Slovak Republicand (VEGA) within the project No. 1/0039/24.

How to cite this article:
Buša, J., Kondela, J., Farkašovský, R. and Jacko, S. (2025), Dangerous Planar Rockfall in an Open Pit: A Case Study from Host'ovce Quarry, Slovakia, *Acta Montanistica Slovaca*, Volume 30 (4), 1018-1033

DOI:
https://doi.org/10.46544/AMS.v30i4.13

Abstract
The structural-geological characteristics and quality of the rock mass influence the design of the quarry opening and the mining method. During mining, the stability of the rock mass often decreases. In some cases, spontaneous rockslides or rockfalls may occur. Such events can endanger workers' lives and damage mining equipment, leading to significant economic losses for the mining company. We present a case from the Host'ovce quarry (limestone mine) in Slovakia, where a rockslide occurred in March 2023, which significantly limited the mine's operations. Using a combination of structural mine mapping and unmanned aerial vehicle (UAV) photogrammetry, the condition and quality of the rock mass were determined, and three categories (C1 – good/fair; C2 - fair/poor and C3 - poor/very poor) were identified in the problematic area of the mine based on the geological strength index with values ranging from 5.0 to 50.0. The unstable rock block found in the lowest quality category, C3 - poor/very poor, of the quarry posed a threat of a possible rockslide. Therefore, safety measures were proposed in the form of a high safety dam to contain the following predicted rockslide. The dimensions of the high safety dam were based on the potential rockslide, with the volume of the selected problematic rock block (marked as X) calculated from a Triangulated Irregular Network (TIN) model derived from unmanned aerial vehicle (UAV) photogrammetry.

Keywords
rock fall, GSI index, UAV photogrammetry, mining mapping, Host'ovce Quarry

Introduction

Open-pit mining is more economically profitable when the mine is deeper and the mining walls are as steep as possible. This causes the slope of the quarry walls to increase in proportion to the amount of waste rock to be extracted (Hustrulid et al., 2013). The slope of the quarry walls is directly dependent on the quality of the rock mass in which it is built. In a weakly cohesive rock mass, it is generally lower than in competent rock. As a result, more waste rock is generated, which means that any increase in the overall angle of inclination (OSA) of the pit walls will have a significantly greater impact on the profitability of mines operating in tectonically reworked and weathered rock masses (Agosti et al., 2021).

A high quarry wall must be stable to protect personnel and machinery used during mining. Porathur et al. (2014) point out that the main hazard recognized in Highwall and Auger Mining projects worldwide is quarry slope collapse. Because it is a remote-controlled mining method, all personnel and most machinery are located at the bottom of the quarry during operation. Catastrophic slope failures have occurred in some Highwall mine shafts where pier stability was critical. Another example is the massive landslide in a copper mine in Utah at the Bingham Canyon open-pit mine near Salt Lake City, Utah, USA, where the landslide triggered several small earthquakes (Pankow et al., 2013). Similarly, an example from the Western Carpathians in Slovakia comes from the Kraľovany quarry, where an unstable slope could potentially trigger a tidal wave in the foothill lake (Kondela et al., 2018).

The issue of ensuring the stability of pitwalls is extensive and depends on factors such as geological conditions, lithology, quality of rock mass, tectonic earthquakes, failures, discontinuities in the rock mass strength, operated mining methods, the height of the benches, and the design of the pitwall (convex, planar, or concave). Newman (1890) describes a profile whose inclination varies with depth, which is better than linear. Hoek and Bray (1977) analysed the stability of some concave circular slopes in cross-section. Guidelines for open-pit slope were designed by Read and Stacey (2009). Stability of the pitwall is described by Brown (2004), Randolph (2011), and Martin and Stacey (2018). Design and optimal slope for pitwall in open mine are represented in studies (Utili et al., 2022; Agosti et al., 2024; Lopez-Pacheco, 2022). Numerical modelling of the pitwall Kacharsky deposit of magnetite ore located in the north of Kazakhstan is described by Sdvyzhkova et al. (2024). Porathur et al. (2014) explain the slope stability assessment approach for multiple seams Highwall Mining extractions. Effect of the width of the gallery of highwall mining on stability of highwall with a numerical modelling approach (Chandar and Kumar, 2014). The slope instability and prevention of landslides with web pillars in coal open pit mines in China (Inner Mongolia Province) were studied using numerical modeling of the instability mechanism of web pillars, as described by Jiang et al. (2022).

Despite advanced methods of modeling pitwall stability, instability still occurs. Instability pitwalls in open mines pose a significant problem, as highlighted by Klenowski and Winter (2017) in their designs for highwall safety bunds in open-cut coal mines. These pitwalls menace the safety of mining machines and cause substantial loss of resources (Chander et al., 2014; 2015).

A similar problem with the stability of the mining floors is in the Hosťovce limestone quarry, Slovakia. The limestones are mined for construction and decorative stone, and for cement production, partly. The quarry is located in the Slovak Karst region with complicated geological and tectonic conditions. In March 2023, the first area rock collapse occurred on the 4th and 5th mine benches, and a secondary area rock fall threatened. Therefore, the Main Mining Office of the Slovak Republic decided to develop a project and implement stabilization elements for safety in the quarry. The article summarizes the solution methodology and a proposal for stabilization measures for safety during mining in the Hosťovce quarry in Slovakia. The implementation of stabilization measures was very difficult because secondary rock was at risk. To identify the risk, detailed structural-geological mapping of the quarry's terrain was applied. The mapping resulted in the identification and demarcation of a potentially dangerous, heavily weathered rock block. We used unmanned aerial vehicle (UAV) photogrammetry to identify potentially dangerous rock blocks.

Geological settings

The site is located in southeastern Slovakia, near the national border with Hungary (Fig. 1). It lies within a karst plateau composed of high-purity limestone, with $CaCO_3$ content reaching up to 99.5%. The exceptional quality of the limestone is associated with sedimentation on a carbonate platform during the Middle Triassic, resulting in the formation of the Gutenstein (Anisian) and Wetterstein (Ladinian) units. The Gutenstein Formation consists of dark grey limestone with abundant calcite-filled joints, while the Wetterstein Formation is characterized by its light grey color and massive structure. The geological sequence also includes various types of carbonates and siliciclastic sedimentary rocks, all part of the Silicicum nappe system. This nappe structure, initially formed during the compressional phase of the Alpine orogeny, was further modified by subsequent Cenozoic tectonic events continuing into the Pleistocene (Mello et al., 1996).

As follows from the described geological settings, the area of the Slovak Karst is tectonically affected and, moreover, consists of rocks for which karstification is a common process of chemical weathering. As a result, the

reactivation of tectonic structures, as well as the formation of some karst structures like caverns, cavities, cracks, and fissures, are very common in such an environment.

The geotechnical parameters of the Wetterstein limestone density from the Hosťovce quarry are identical to the limestone from the Včeláre mine: φ = 2.706 kg.m^{-3}, porosity n = 0.20% and deformation modulus $Edef$ = 81.0 MPa with a Poisson number υ = 0.27 (Holzer et al., 2009).

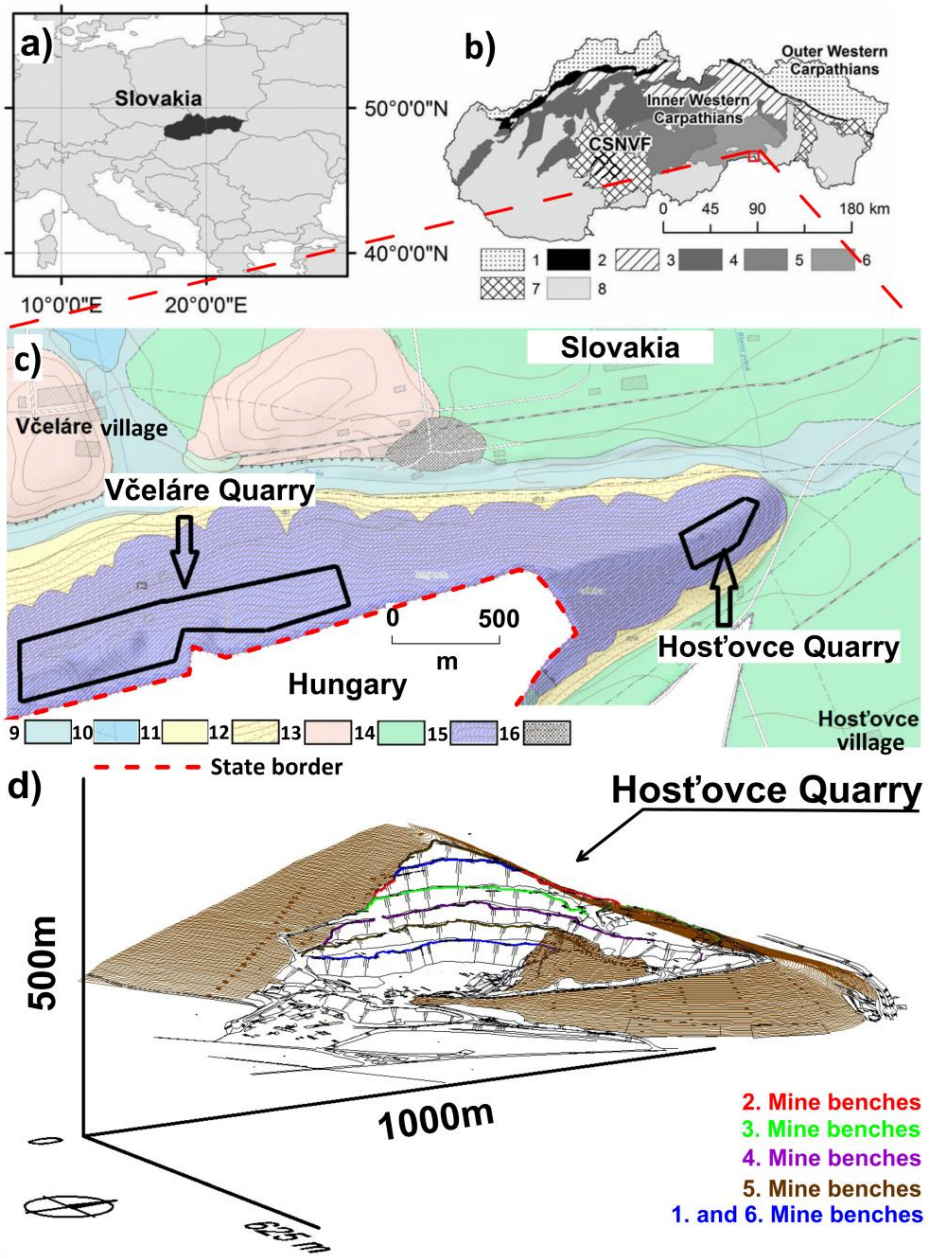

Fig.1. Location of the study area in Central Europe (a); main tectonic units of the Western Carpathians in Slovakia and location of the Slovak Karst/Gemer belt (b): 1– Flysch belt, 2– Pieniny Klippen belt, 3– Inner-Carpathian Paleogene, 4– Tatra-Fatra belt of core mountains, 5– Vepor belt, 6– Gemer belt, 7– Neogene volcanics and 8– Neogene basins; general geological setting of the study area geology of study area (c) (edited by Mello et al. 1996)): 9- Quaternary: fluvial sediments (gravel and mud), 10– organic sediments-peat, 11– deluvial-fluvial sediments- outwash loams, sandy loams, 12– deluvial sediments - screes mostly loamy-stony, 13– fluvial sediments - floodplain, 14-proluvial sediments-mud with sandy gravel, 15 - Mesozoic-wetterstein limestone and 16-Antrhropogenic material and 3D view Hosťovce mine with becnhes - status as the 05/2023 (d).

Limestones are layered, with a thickness ranging from 0.3 to 1.5–2.0 meters. The stratification generally follows an NE-SW direction with a slight monocline inclination of 10-20° towards the NW. The structural features of the quarry are primarily influenced by fractures in the NZ-SE and N-S directions, with sinistral or dextral displacements. The second system is represented by NW-SE fractures, which show only subsidence activity (Mello et al., 1996).

Material and Methods

In order to ensure the safety of the machines and miners and to propose remediation measures, it was necessary to identify and characterize the risky part of the quarry. After the rockfall of parts of the bedrock, part of the quarry became completely inaccessible. Therefore, a combination of three methodological procedures was chosen to identify the risky part of the quarry and its characteristics. Before using the individual methods, the condition after the rockfall was documented.

Structural mining mapping and geological documentation associated with the identification of karst phenomena.

Structural mining mapping and geological research involved measurements and documentation at various quarry levels using geological compasses in areas where access was safe. The location of each measurement was made at safe locations (Fig. 2).

Fig.2. The basic mining map with field documentation points in the Hosťovce Quarry. Topography is sourced from the basic mining plan (chief mining surveyor Ing. Thuróczy).

The result is stereograms that determine the trajectories of fault lines based on orientation, dip length, and fracture spacing. The resulting set of structural data with the deposition orientation set to 0–360 degrees is displayed in a stereo grid of hemispheres. Stereograms are an important tool in structural-geological mapping,

allowing visualization and analysis of the orientation of geological structures such as layers, fault planes, and other rock textures (Call 1992). These diagrams provide a spatial representation of data obtained from field measurements and facilitate the interpretation of geological processes and structural patterns (Nicholas and Sims 2000).

UAV photogrammetry and rock block analysis

Agisoft PhotoScan software then processed the 180 images. When images were aligned and tie points generated, the Structure-from-Motion (SfM) algorithm (Snavely et al., 2008) was used to build model geometry (image orientation and exterior orientation). Ground control points provided spatial georeferencing and accuracy estimation, and orthophotos, and a colored point dense cloud of 8,254,575 points was generated for DTM calculation. The terrain model with 9,06 cm pixel resolution and 2 cm vertical and horizontal accuracy was thus generated. Individual parts of the DTM creation and the orthophotomosaic are shown in Figure 3a-d.
The volume calculation of the selected rock block was carried out in AutoCAD CIVIL 3D using the Volumes Dashboard function. This function calculates the volume based on TIN (triangulated irregular network). The detailed processing of geological objects is dedicated to the CAD system described by Blišťan and Grinč (1998).

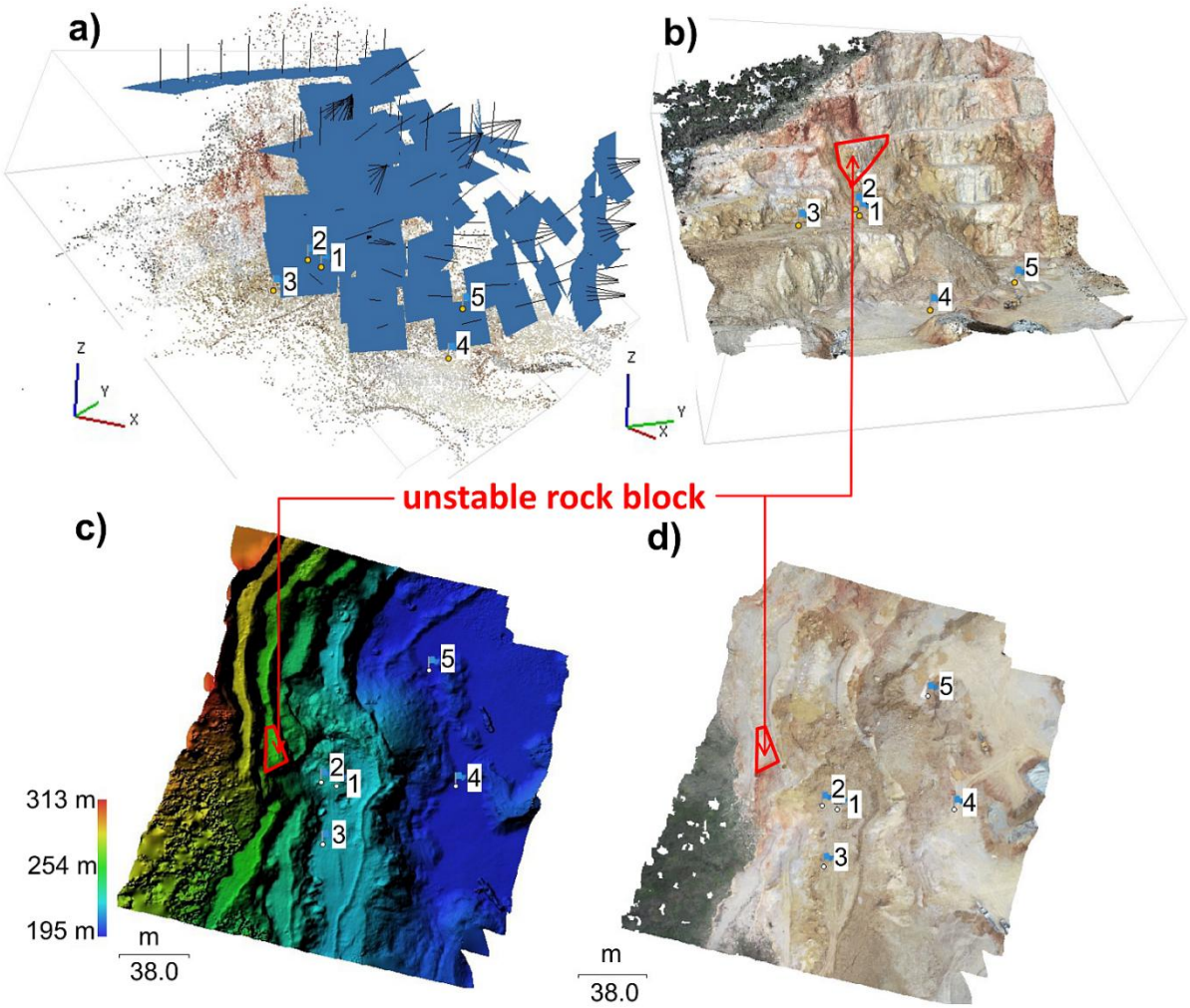

Fig.3. The tie points 74 688 and camera alignment and flight paths above the pit wall, with flying heights of 35 to 65 m above ground level, respectively (a). The dense cloud with 8,254,575 points (b). Visualization of digital terrain model (c), orthophoto mosaic (d).

GSI classification – estimate of rock mass properties

Rock masses consist of intact rock that is intersected by various geological discontinuities such as joints, bedding planes, veins, shear zones, and faults, forming a complex structural system (Narimani et al., 2023). We used the Geological Strength Index (GSI) charts for rock mass classification, by Hoek and Marinos (2000). The Geological Strength Index (GSI) is based on an assessment of the lithology, structure, and condition of discontinuity surfaces in the rock mass. It is estimated through visual examination of the rock mass exposed in

surface excavations. The GSI index, by combining two fundamental geological parameters—the blockiness of the mass and the condition of discontinuities—accounts for the main geological constraints that govern rock formation. As such, it is both geologically meaningful and practical for assessment (Hoek, 1994). Hoek and Bray (1977) proposed the geological strength index (GSI) based on the visual impression of the rock mass structure. The charts describe the structures and surface conditions of rock mass, showing a decrease in interlocking of rock pieces and surface quality from 0 to 100%, where 0% represents very poor conditions and 100% represents very good conditions.

Before estimating the assessment in the inaccessible part of the quarry, the structural state of the rock massif in the accessible part of the Hosťovce quarry was identified and described. A mining geological-structural map was created. The mapping results provided basic lithological, structural, engineering-geological, and geotechnical information for the assessment of the massif. After using photogrammetry, the information obtained in the field during the mapping was interpreted in the inaccessible area of the Hosťovce quarry.

Results

Determining the cause of instability

The geological structure within the mine is highly complex and directly affects the stability of the pit walls. The first signs of instability on the 4th and 5th mine benches appeared in March 2023, when a rockfall was triggered. The shear zone and the accumulated material from this initial event are shown in Figure 4a and in Figure 5 (Locations No. 6 and No. 4).

The rockfall from the pit walls is in another part of the mine, highlighted by No. 1, 2, and 3 (these rock blocks are approximately 1.0-2.0 meters in size), and the primary safety bunds are marked as No. 5. The shear zone of the landslide in March 2023 is marked as No. 6, and the talus accumulation zone is marked with No. 4 in the Figure 5.

Structural mining mapping and analysis

Half of the exposed mine pit walls could not be accessed due to safety concerns. Several access routes through mine benches III, IV, and V to the mine pit walls in the south part of the quarry are not possible, as shown in Figure 4. In the area of the rockfall, in the southern part of the mine, movement on the levels is prohibited. The dataset of structural-geological analysis was created from 76 measurements. The measurements were performed at 10 documentation points in the accessible part of the quarry shown in Figure 6. The selected 10 documentation points include all clearly identifiable structural, lithological, and karst phenomena and their relationships (Fig. 2).

Structural analysis was performed to clarify the geometry and kinematics of the faults along the studied fault sections, as well as their possible influence on the position of the rockfall. Secondary structures, fault features, and fractures were identified during the documentation. Occasionally, primary structures—layering surfaces—were preserved in block fragments. The layering surfaces were tilted, with distinct interlayer movements. Interlayer surfaces were reinforced with light gray calcite. At the contact with fault structures, the layering surfaces were flexurally bent or even uplifted. Based on the processing of the documentation results and the graphical representation of the fault structures in the Hosťovce quarry, it is clear that tectonic structures with moderate to steep dips prevail statistically, with a preference for directions in the NE-SW and ENE-WSW orientations (Fig. 6a). In these directions, oblique dips dominate over oblique displacements. Occasionally, dextral displacements were identified in this direction. Other directions of fault tectonic structures are minor, but their dips exceed 40.0°.

The dominant structural system on I and II mine benches consists of planar fault structures, occasionally with linear elements, oriented in the NE-SW direction with a moderate to steep dip towards the SE (Fig. 6a). These planar elements in most cases represent secondary fault structures, occasionally with preserved striations of movement in brittle conditions. The faults have the character of dips or oblique (dextral) displacements (Fig. 6b). In these structures, tectonic breccias with angular limestone fragments are irregularly situated, cemented with carbonate mineralization or reinforced with clayey material.

In cases where fault surfaces are part of karst cavities or border them, they are usually smoothed (corroded), often covered with sinter coatings of varying thickness, sometimes with karst decorations. These areas may also represent the edges of karst cavities, which may be filled with sandy-loamy-clayey poorly consolidated sediment, or even solid sedimentary rock. The solid sedimentary rocks in the cavities are characterized by obliquely deposited layers of sandstone and siltstone. Their oblique orientation is the result of tectonic movements along the aforementioned fault structures. The cavities also contain disordered material of boulder-sized breccias cemented by unconsolidated clayey fill. Over time, after the formation of structures with this type of fill, the influence of climate or mining (technical seismicity) causes the boulders to become loose from the fill. They fall spontaneously and descend to lower platforms by landslide or collapse, and temporarily stop. Alternatively, they may collapse onto the lowest VI mine benches (Fig. 4a).

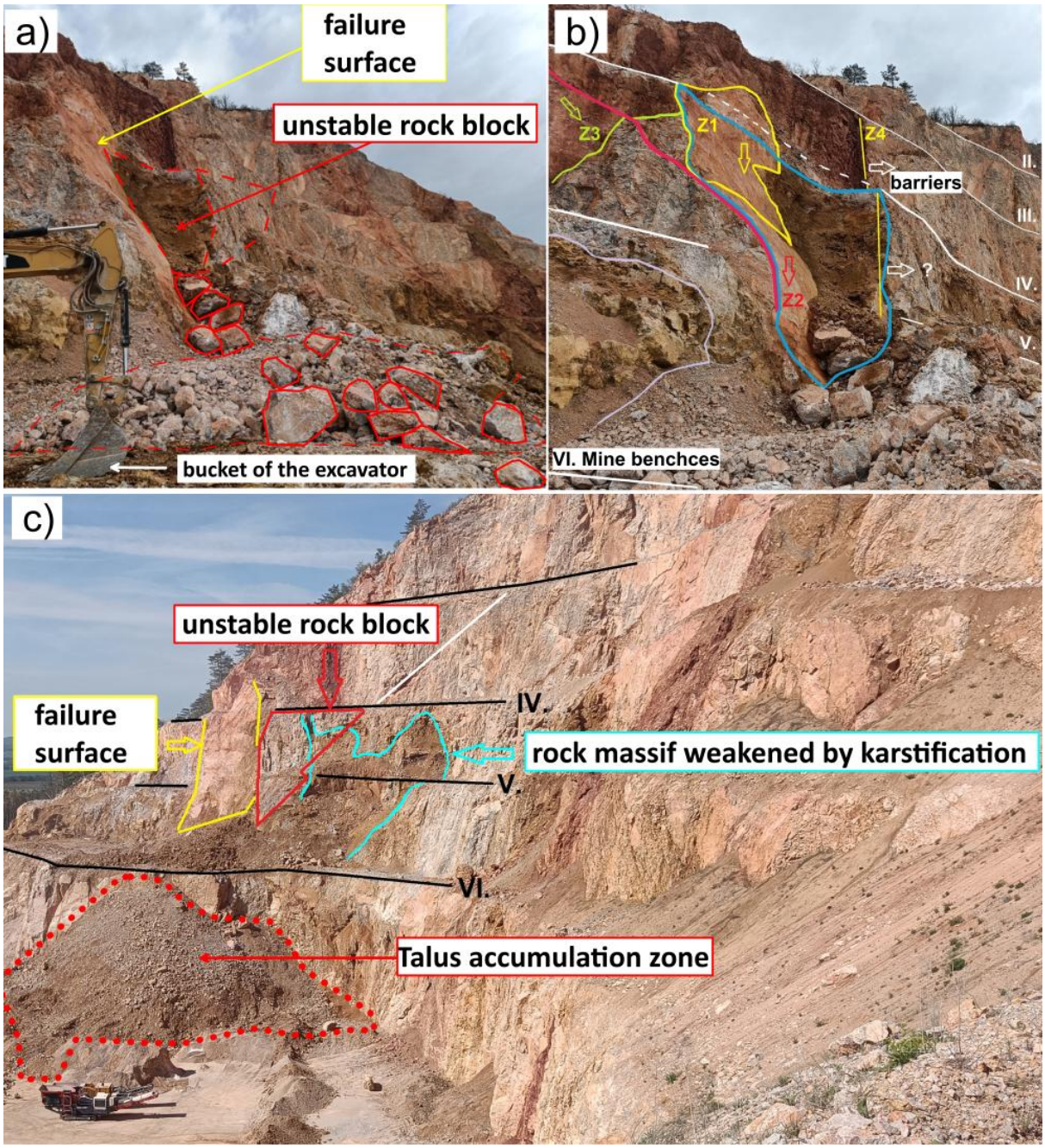

Fig.4. Documentation after the rockfall between mining floors III and VI of the quarry. Debris and rubble cone from the rock collapse from the III. and IV. Mine benches with the position of boulders captured on the lower V. mine bench. (a) Schematic of the succession of tectonic fault structures (fault planes – youngest red – Z2, older yellow – Z1, Z4 and oldest green – Z3) and karst phenomena (breccia and karst zone – blue), which, due to their spatial position and mutual interaction in the rock massif, caused the collapse of rocks. (b) The orientation of the quarry wall, which is almost parallel (in direction and inclination) to the tectonic structures (red, yellow) bordering the karst zone with karst fillings, significantly contributed to this. A significant factor in reducing the stability of the massif was also the excavation at the IV. and V. mining levels, which undercut and exposed the zone of breccias and intensive karstification. State after the rock collapse and the delineation of the unstable rock block (red) in the massif. This is a block in the massif, tectonically bounded, with partial representation of karstified rocks (blue). (c) A view from the accessible part of the quarry to the inaccessible part of the quarry after the rock fall.

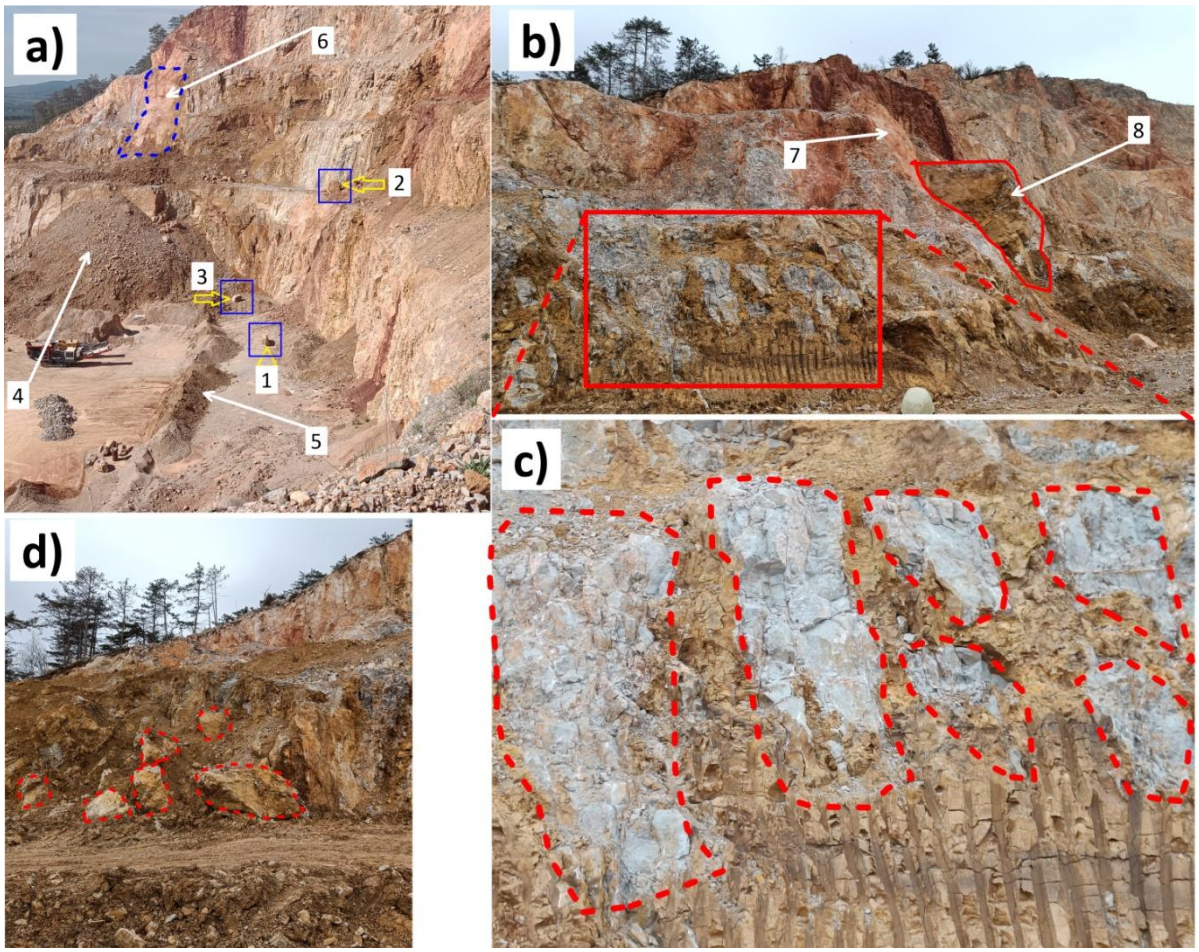

Fig.5. The rockfall in March 2023 and complicated geology. The location of the rock fall in March 2023 (a): No. 1, 2, and 3 are rock blocks from the pit walls, each with a size of 1-2 meters; No. 5 is the primary safety bund; No. 4 is the accumulation part, and No. 6 is the shear zone of the first rock fall in March 2023. Potentially dangerous rock block (b) marked with No. 8, and the shear zone of the first rock fall, marked as No. 7, along with details on the complicated geology. Rock blocks of limestone (size 15-20 meters) with a karstification zone on clay with medium or high plasticity form a collapsed cavern system in the 1st mine benches (c). Rock blocks (collapse breccia) at the edge of the south part of the mine (d). Loose, weathered, uncemented carbonate breccia (limestone blocks) with clay-lime cement.

In addition to the prevailing northeast-southwest directions, the rock massif contains rarely developed older fault structures with very steep inclinations and almost east-west orientation (Fig. 7c). These structures are often accompanied by breccia zones of varying thickness along their course. The breccia zones are distinctly karst. Sinter deposits of various shades of gray, brown, and red are common on the surfaces. The cementation of the tectonic breccia is heterogeneous and is sometimes cemented by calcite, while in other areas it is cemented only by clay. These are zones of reduced stability in the rock massif with a higher probability of collapse of rock blocks. The formation and development of the block structure in the Hosťovce Quarry are documented by the identified mutual relationships of fault structures in section IV (Fig. 7d). Relative temporal relationships between the steeply inclined structures in the E-W and NE-SW directions are revealed here.

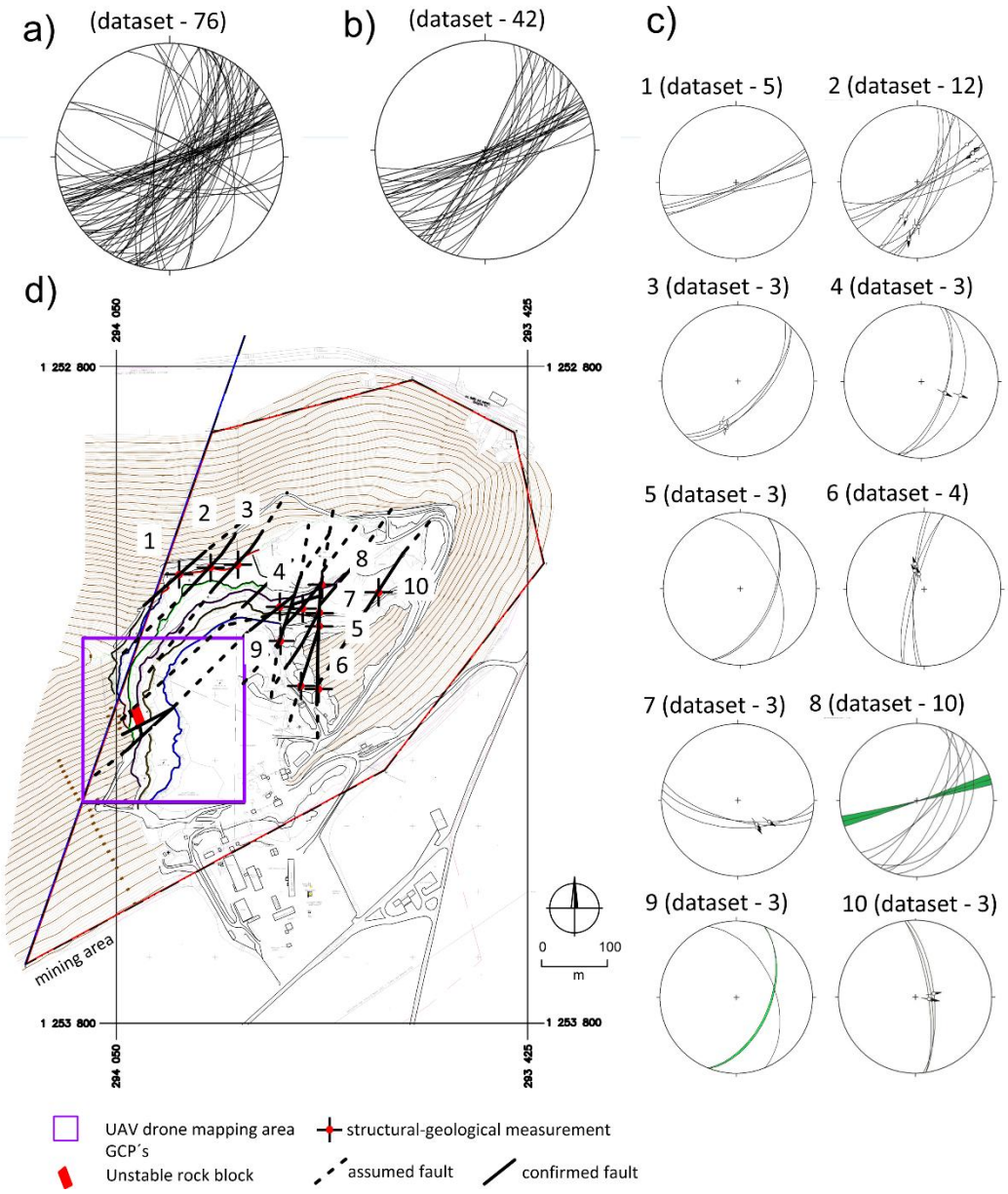

Fig.6. Map of the study area in the quarry. Great circles in stereoplots illustrate fault data. The tectonogram of all measured fault structures in the Hostovce mine (a). Structural elements dominating the upper mine benches (I, II, III, IV, V) of the Hostovce mine are fault planes oriented in the NE-SW to ENE-WSW direction, with a moderate to steep dip towards the SE (b). The individual tectonograms (c). The map of structural measurements with the UAV mapping zone (d).

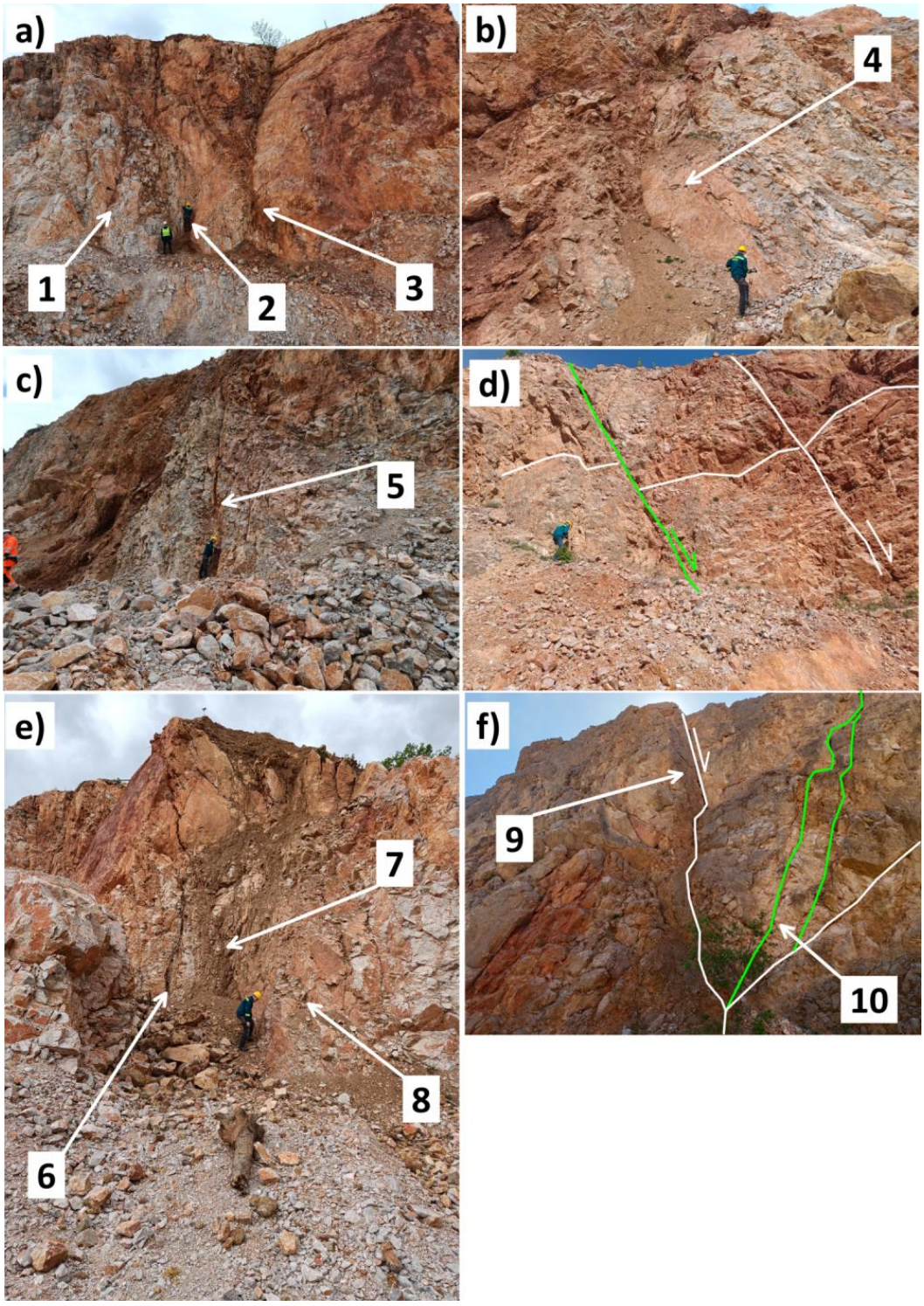

Fig.7. Documented structures (documentation points 1-3), wall of the 0th mine bench. Significantly karstified surfaces, partially covered with sinter, with coatings of Fe and Mn oxides. Between fault structures 1 and 3, a brecciation zone is developed, cemented with clay, with an oppositely oriented fault 2 (a). Fault structure on the 1st becnches, dextral displacement, bounding a zone of intensely karstified, poorly cemented tectonic breccia cemented with brown clay, containing limestone boulders up to 1m³ (bottom right corner) (b) An older, steeply inclined fault structure with a nearly E-W orientation, filled with sinter and reddish-brown clay, intersecting the brecciation to crushing zone at the 0th benchces (on the left) (c) The succession of fault structures documenting the unblocking of the massif. An older strike-slip and dip-slip fault structure is intersected by younger NE-SW dip-slip fault structures (d) The younger dip-slip N-S structure 1 terminates the older NE-SW structure, bounded by fault planes 2 and 3 on the II benches (e) The succession between the younger dip-slip N-S structure, which terminates the older NE-SW structure (green), at the level between the IV and V mine benches (f).

The genesis and evolution of the block structure in the Host'ovce mine are documented by the identified mutual relationships of fault structures at the IV mine benches (Fig. 7d). Relatively temporal relationships between steeply inclined structures in the E-W direction and NE-SW direction are exposed here.
In the E-W direction, oblique thrust structures or structures of oblique waves were identified, which are intersected by younger subparallel asymmetric wave structures in the NE-SW direction. Asymmetric wave faults are truncated, filled with sinter deposits of various colors or younger calcite mineralization. At the same time, we can observe the relationship between the wave structures in the NE-SW direction and the youngest wave faults S-S at the level between the IV. and V. benches. The mutual gradual relationship between the youngest wave structures S-S and older NE-SW structures can be observed in several places on the walls of the levels (Fig. 7 c/f). The fillings of the youngest structures of the inclined fault S-S are characterized by a high degree of beauty of tectonic breccias cemented by clay. Unlike other structures, they have a distinct red to brown color. Only rarely are sinter coatings found in the fillings. In general, it is a rock massif with a blocky geological structure. It is formed by irregular micro and macro blocks of carbonate rocks. Individual blocks are affected by varying degrees of brecciation and karstification.

Based on the course and intersection of dominant fault structures, the density of fractures, brecciation zones, and the intensity of karstification, a tectonic block with a higher risk of landslides or rock collapse was selected.

Rock Mass Classification based on GSI index

Based on structural mining mapping, geological documentation, and UAV photogrammetry, we selected 10 blocks with varying discontinuity surface conditions in the rock mass. These conditions were estimated through visual examination of the rock mass exposed in the evaluated part of the quarry. The spatial location of the individual geologically and geomechanically distinct rock blocks is shown in Figure 8a, and their position in GSI charts is shown in Figure 8b.

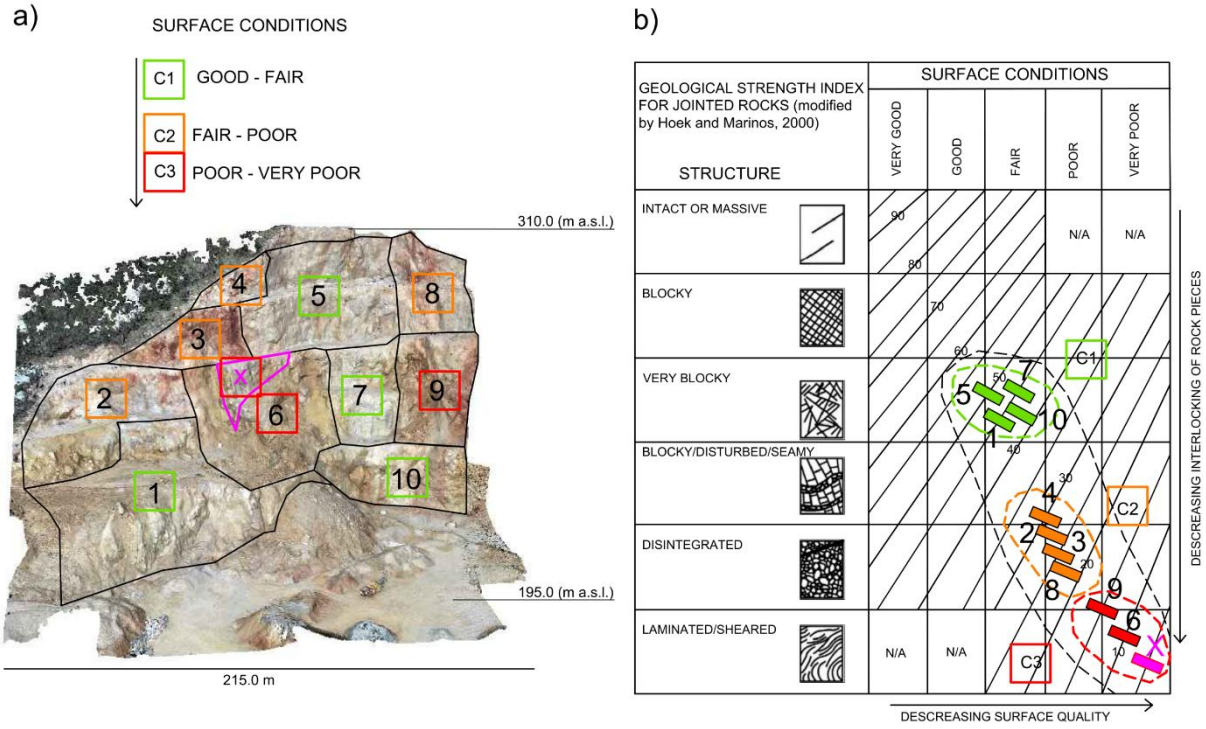

Fig.8. Classification of rock mass blocks in groups C1–C3 (from green to red), including unstable rock blocks (magenta), is based on the Geological Strength Index (GSI) for jointed rocks, as modified by Hoek and Marinos (2000). The categories of block groups C1–C3 are shown in the UAV mapping zone in the Host'ovce quarry (a), and the GSI chart (b).

Individual rock blocks were classified based on the GSI classification (Fig. 8b). According to this classification, three categories—C1 (green), C2 (orange), and C3 (red)—were identified (Table 1), considering the future potential for weathering, stability, and rockfall risk. A total 3D area of 44,876.0 m², derived from UAV mapping, was classified.

Group C1 (green) consists of rock blocks No. 5, 1, 7, and 10, with a GSI index ranging from 43.0 to 48.0%. Group C2 (orange), composed of rock blocks No. 4, 2, 3, and 8, has a GSI index between 23.0 and 28.0%. The final group, C3 (red), includes rock blocks 9, 6, and X, with a GSI index ranging from 8.0 to 13.0%. The total

weighted average GSI index for the classified zone is estimated at 30.0–35.0%. Summary values from the GSI index charts are presented in Table 1.

Tab. 1 Classification of rock blocks from UAV mapping based on GSI index.

Categories	Blocks	GSI [%] interval	GSI [%] Value	Area 3D [m2] 44876,00	Area 3D [%]	Weighted average - CSC GSI [%]	Total weighted average GSI [%]
C1	Block 5	47.50-52.50	50.00	6289,90	52.29	45.95 [43-48]	33.1 [30-35]
	Block 1	42.50-47.50	45.00	10912,66			
	Block 7	42.50-47.50	45.00	2624,30			
	Block 10	40.00-45.00	42.50	3639,31			
C2	Block 4	27.50-32.50	30.00	923,85	25.05	26.01 [23-28]	
	Block 2	25.00-30.00	27.50	5381,82			
	Block 3	22.50-27.50	25.00	2259,66			
	Block 8	20.00-25.00	22.50	2675,13			
C3	Block 9	12.50-17.50	15.00	3481,53	22.66	11.24 [8-13]	
	Block 6	7.50-12.50	10.00	5732,43			
	Block X	2.50-7.50	5.0	955,41			

From the perspective of the highest degree of tectonic damage and the most intensive weathering, Block X was selected. It has the lowest GSI index and experienced material fallout several days after the initial rockfall. Therefore, block X was classified as unstable and the most hazardous.

UAV photogrammetry and rock block analysis with proposal for safety measures

The calculation used Surface 1, created from a POINT CLOUD (generated from UAV photogrammetry), trimmed for the BLOCK (Fig. 9 a/b/c). The rock block consisted of a point cloud with a total of 38,742 points. The block boundaries were created based on geological-structural documentation and surveying data. These boundaries formed Surface 2, which was used in the comparison function of the Volumes Dashboard. By comparing the created surfaces, Surface 1 and Surface 2, the volume of the selected rock block was determined to be 3,099.59 m³. A total of 76,597 triangles of the irregular network were generated, based on which the volume was calculated.

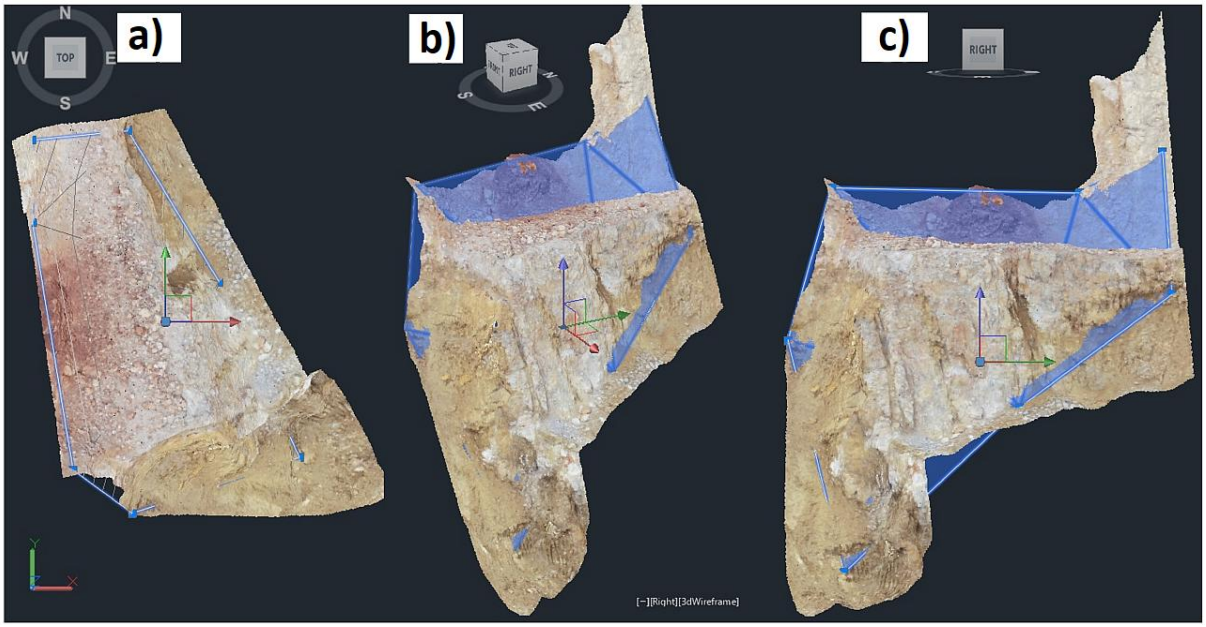

Fig.9. Unstable rock block – different views unstable rock block (e) - top view, (f) - isometric view, (g) - side view Visualization in AutoCAD CIVIL e-g.

The primary safety measure was constructed after a rockfall from March 2023 on the platform of the 5th mine bench (Fig. 10c), designed to catch individual falling boulders from the overlying rock collapse. Similarly, the volume of the selected block was calculated, and using TIN in AutoCAD CIVIL 3D, the volume of the existing bed on the 5th mine bench was computed to be 2,631.92 m³. Given the height of the collapse, rock falling may come from heights exceeding 40.0 meters. At the crest of the 6th mine bench, it is necessary to build a protective hightwall safety bund. This embankment should reduce the potential scatter of boulder fragments when a boulder falls from height onto a boulder resting on the bed. The dimensions of the highwall safety bund are 50.0 meters in length and 5.0 meters in height (Fig. 10 c/d).

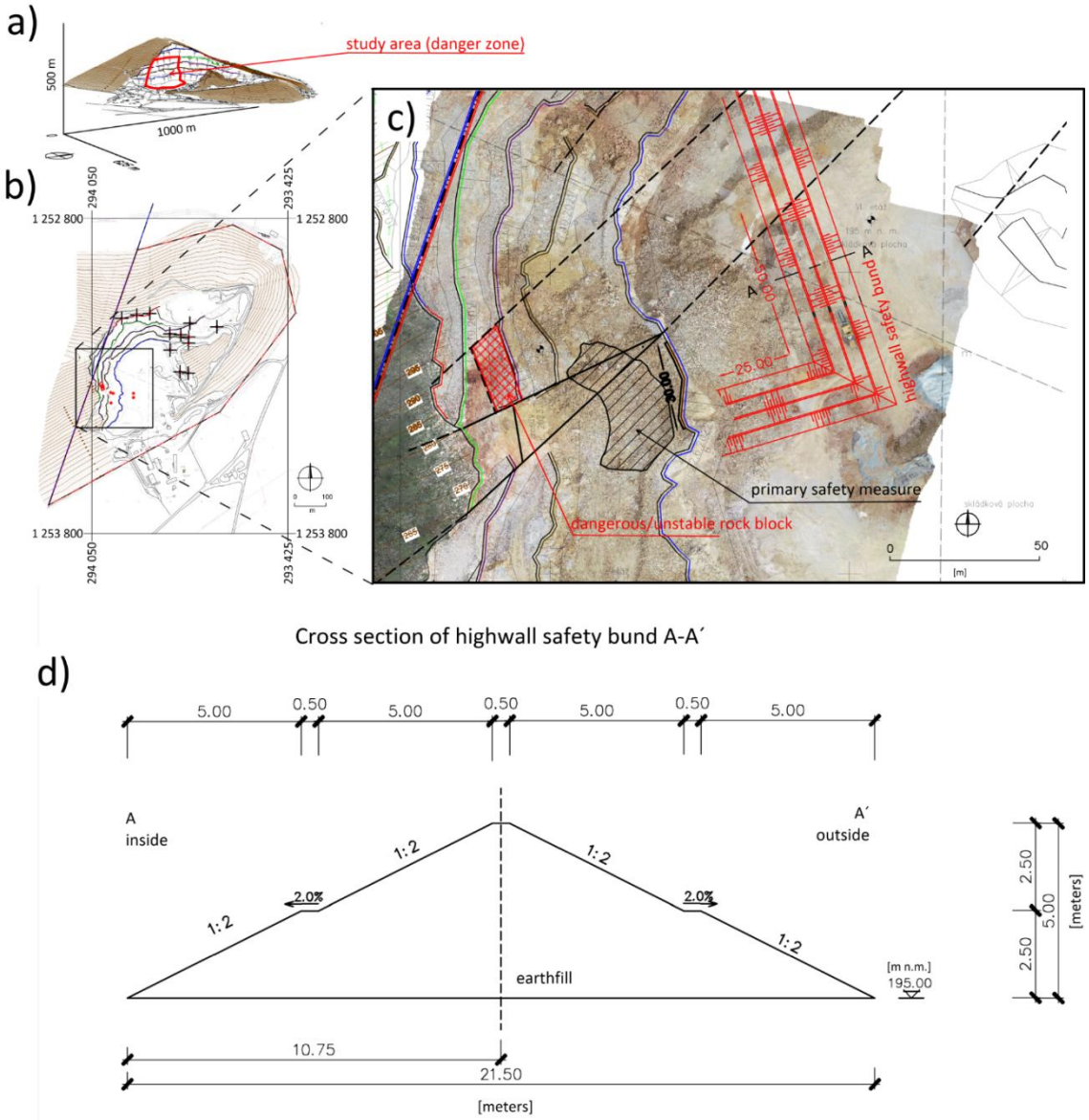

Fig.10. The selected rock block, with a volume of 3,099.59 m³, is bounded by blue surfaces between the IV and V mine benches, and its stability within the rock mass is uncertain following the collapse.

Discussion

Growing public concern about the impact of geohazards on technology and quality of life has accelerated the development of advanced remote sensing technologies. Today, society can detect landslide movements smaller than a centimeter from space and create detailed terrain models using small drones. However, a thorough understanding of slope deformation requires a holistic approach that integrates in-situ measurements, assesses triggering mechanisms, employs interdisciplinary methods in morphological studies, continuously monitors and analyzes slope movements, and provides accurate risk assessment (Chae et al., 2017). One such method is UAV photogrammetry, which was used in the Jastrabá quarry by Kovanič et al. (2017). They concluded that it is a fast and relatively accurate method for capturing mining activities and documenting the mining process. Kovanič and

Németh (2013) applied geodetic methods (specifically, terrestrial laser scanning, TLS) to model dolomite quarry walls and rock outcrops and used the data in structural analysis in the Sedlice quarry in Slovakia. Uysal et al. (2015) highlight the significant limitations of using a total station to document complex morphological features and for detailed mapping of steep and irregular mine pit walls. Buša et al. (2020) used UAV photogrammetry to detect movement in the Svätý Anton landslide (central Slovakia). The presented study points to the justification for using UAV photogrammetry to map the inaccessible rock massif of the Hosťovce quarry.

Structural mining mapping and analysis confirm that the rock collapse occurred in the western part of the Hosťovce quarry, where the mining pit walls run in a northeast-southwest (NE-SW) direction. Fault structures of various origins and generations tectonically disrupt the mined rock massif. Quantitatively, the system of subsidence and oblique subsidence faults predominates, oriented from NE-SW to S-N, with a moderate to steep dip towards the southeast. Numerous irregular zones of tectonic breccias have formed between the individual structures. Because surface water infiltrated the massif along these structures, all of them have become karstified. The intensity of karstification varies widely; generally, the closer to the surface, the more intense the karstification. Cavities (endokarst) have primarily formed along the fault planes, often filled with tectonic breccia and clay. The degree of cementation of these fillings is highly variable. Changes in the character of the filling and its cementation can sometimes be observed within a single tectonic line, depending on the varying degree of calcification of the breccia-clay filling.

New calcite veins or druses can be observed within the clayey-sandy filling in several instances. In the bench's pit wall, where most of the rock material collapsed, collapse breccia is even preserved. Its filling consists of boulders larger than 1.0 m³, cemented by a calcified clayey-sandy matrix. The closer the collapse breccia is to the surface, the lower the degree of cementation. The most intense and widespread endokarst phenomena (collapse breccias, karst cavities filled with breccias, or even layers of sedimentary rocks) are found between mine benches III and V of the quarry. In this quarry area, an intensively disturbed and weathered block of rock massif with an increased risk of collapse was identified. Using UAV photogrammetry, the unstable rock block was outlined. Based on its boundaries, it was possible to determine its volume parameters. After identifying these parameters, safety measures were devised for the quarry.

UAV photogrammetry and structural mining mapping were useful in classifying limestone rock mass for the GSI index, with values ranging from 30.0 to 35.0 across three categories C 1- C 3 (Tab. 1). According to Bögöly and Füzesi (2021), the GSI value for dolomites in Csákvár, Northern Hungary—located beneath the Vértes Mountains and primarily composed of the Upper Triassic (Carnian to Rhaetian) dolomite—is 35.0. Špago and Jovanovski (2019) reported GSI values of up to 70.0 for carbonate rock mass classification. Tsiambaos and Saroglou (2010) classified limestone in Greece with GSI values ranging from 20.0 to 65.0. By Wijaya et al. (2013), the estimated GSI values for the rock mass quality in the cavity layer zone of the limestone quarry in the Sale District, Rembang Regency, Central Java Province, Indonesia, range from 32.0 to 39.0, indicating poor rock mass quality.

With a poor-quality rock mass (GSI values between 30.0 and 35.0), the volume of the existing high safety bund at the V mine benches (Fig. 10c – primary safety measure), calculated using AutoCAD Civil 3D and TIN modeling based on UAV photogrammetry, was 2,631.92 m³. This volume was found to be insufficient, leading to the design of a higher safety bund at the VI mine bench. Considering the height of the potential collapse, rock falls (such as from Block X, which has a GSI value as low as 7.50) could occur from heights exceeding 40.0 meters. Therefore, a highwall safety bund should be constructed (Fig. 10d) at the crown of the VI mine benches to reduce the potential spread of rock fragments when blocks fall into the safety bunds.

However, it is essential to note that in the event of a sudden collapse of the selected block, the loosened rock volume may exceed the capacity of the existing high safety bunds to contain it. Additionally, the current bedding plane does not extend beneath the entire selected block, which is compromised in terms of stability. As a result, the volume of rock that the safety bunds can capture is smaller than the volume of the selected block. In highwall mining, it is crucial to conduct a stability assessment of the slope before extraction activities, particularly when multiple layers are mined in a vertical sequence. Slope stability must be maintained throughout each phase of the operation. It is evident that the web cuts planned within each seam can significantly impact the overall stability of the highwall. The stability of quarry pit walls is directly dependent on the quality of the rock mass, and a comprehensive structural analysis of the rock mass is required before the commencement of excavation work. It is also necessary to monitor the quality of the rock mass during extraction in order to prevent unexpected events and risks to life and property.

The rock mass quality in the extraction area can vary significantly, as observed in the Hosťovce quarry, where GSI index values ranged from 2.50 to 52.50%. The structural and geological characteristics of the rock mass influence this variability. Based on structural-geological mapping combined with UAV photogrammetry, three zones (C1–C3) were identified according to rock mass quality: C1 (43.0–48.0%), C2 (23.0–28.0%), and C3 (8.0–13.0%). The highest-quality section of the rock mass is zone C1, with the highest GSI index and a 3D surface area of 23,466.13 m², representing 52.29% of the mapped area. Zone C3, with the lowest GSI index, covers an area of 10,169.37 m², or 22.66%. This zone represents areas with marginal rock mass stability, which may be disturbed

by extraction activities (technical seismicity) and could lead to sudden rock collapses (e.g., Block X). To mitigate this risk, high safety bunds measuring 5.0×50.0 meters were proposed on the VI. mine bench to intercept falling rock material.

This is one of the critical parameters affecting safety in mining operations. Therefore, if future extraction is considered below the elevation level of the plateau on the VI mine bench, both the width of the plateau and the height of the safety bund on this mine bench must take this risk into account. When planning the orientation of future quarry pit walls, it is important to avoid alignment with the main tectonic structures trending NE-SW and N-S, especially extraction along fault zones with poorly consolidated (karstified) infill. In the interest of quarry safety, maintaining access routes beneath each bench face would be beneficial. This would allow for controlled release or removal of loosened boulders resting on the mine benches. Such a measure would reduce the risk of unexpected sliding or collapse of rock blocks across multiple benches during operation. Consequently, it would also minimize the potential for unpredictable rock fragment dispersion of the sixth bench, thereby reducing the risk to personnel.

Conclusions

The quality of the limestone rock mass can vary significantly during mining; in the Hosťovce quarry, GSI index values ranged from 2.50% to 52.50%. This variability is primarily influenced by (a) structural and geological conditions that temporarily modify the rock mass, and (b) the impact of mining, which reduces the stability and cohesion of the rock mass.

In the limestone quarry, three quality zones were identified (C1–C3): C1 (43.0–48.0%), C2 (23.0–28.0%), and C3 (8.0–13.0%). Zone C1, with the highest GSI index and a 3D surface area of 23,466.13 m², accounts for 52.29% of the mapped area. The Wetterstein limestones are fragmented by several systems of faults and joints without clay infill and show no visible karstification on the fault planes. In this zone, the fractures are macroscopically striated with calcite, and dilatant veins and breccia are common.

Zone C3, with the lowest GSI index, covers an area of 10,169.37 m², representing 22.66% of the mapped surface. This zone includes areas with marginal rock mass stability, which may be affected by mining activities (technical seismicity) and could result in sudden rockslides (e.g., block X). To mitigate this risk, six high protective dams, each measuring 5.0×50.0 meters, have been designed to intercept falling rock material.

When planning the orientation of future quarry pit walls, it is crucial to avoid alignment with major tectonic structures trending NE–SW and N–S, particularly when mining along fault zones with weakly consolidated (karst) infill. Additionally, continuous monitoring of the rock mass quality is necessary during mining operations to prevent unexpected events and reduce risks to life and property.

References

Agosti A., Utili S., Gregory D., Lapworth A., Samardzic J., Prawasono A. (2021). Design of an open-pit gold mine by optimal pitwall profiles. *CIM Journal*, 12(4), 149-168. DOI: 10.1080/19236026.2021.1979382.

Agosti A., Cylwik S., Utili S., (2024). *International Journal of Mining, Reclamation and Environment*, DOI: 10.1080/17480930.2024.2387988.

Blišťan, P., Grinč, A. (1998). Processing of the geological documentation using CAD systems and GIS. *Acta Montanistica Slovaca*, 1, 157-167.

Brown, ET. (2004). Geomechanics: The critical engineering discipline for mass mining. In: A. Karzulovic & M. Alfaro (Eds.), *MassMin: Proud to be Minders: Proceedings*, 21–36.

Bögöly, G., Füzesi, F. (2021). Comparison of the probabilistic and deterministic slope stability analysis of a dolomite quarry in Hungary. In book: The Evolution of Geotech - 25 Years of Innovation. DOI: 10.1201/9781003188339-24.

Buša, J., Rusnák, M., Kušnirák, D., Greif, V., Bednarik, M., Putiška, R., Dostál, I., Sládek, J., Rusnáková, D. (2020). Urban landslide monitoring by combined use of multiple methodologies - a case study on Sv. Anton town, Slovakia, *Physical Geography*, 41, 2, 169-194, DOI: 10.1080/02723646.2019.1630232.

Call, RD. (1992). Slope Stability. In Hartman (ed.), *Mining Engineering Handbook* 2nd ed. vol. 1, Soc. for Mining, Metallurgy, and Exploration, Littleton.

Chae, BG., Park, HJ., Catani, F., Simoni, A., & Berti, M. (2017). Landslide prediction, monitoring and early warning: A concise review of state-of-the-art. *Geosciences Journal*, 21, 6, 1033–1070.

Hoek, E. (1994). Strength of rock and rock masses. *ISRM News J*, 2(2), 4–16.

Hoek, E., Bray, J. (1977). *Rock Slope Engineering*. The Institution of Mining and Metallurgy, London.

Hoek, E., Marinos, P. (2000). Predicting tunnel squeezing. Tunn. Tunn. Int. 2000, 32, 45–51.

Holzer, R., Laho, M., Wagner, P., Bednarik, M. (2009). Engineering Geological Atlas of Rocks of Slovakia. *Štátny geolologický ústav Dionýza Štúra Bratislava,* ISBN 978-80-89343-29-4.

Hustrulid, W., Kutcha, M., & Martin, R. (2013). Open pit mine planning and design. CRC Press.
Chandar, KR., Kumar, BG. (2014). Effect of width of gallery of highwall mining on stability of highwall: a numerical modelling approach. *International Journal of Mining and Mineral Engineering.* 5(3), 212–228.
Chandar. KR., Hegde, C., Yellishetty, M. (2015). Classification of stability of highwall during highwall mining: a statistical adaptive learning approach. *Geotech Geolog Eng*, 33, 511–521.
Jiang, J., Zhang, Z., Wang, D., Wang, L., Han, X. (2022). Web pillar stability in open-pit highwall mining. *nternational Journal of Coal Science & Technology.* 9, 12.
Klenowski, G., Winter, S. (2017). Designs for highwall safety bunds in open cut coal mines, *AusIMM Bulletin*, 76-78.
Kondela, J., Prekopová, M., Budinský, V., Pandula, B., Ďuriška. I. (2018). The importance of seismic methods application for geological reconstruction of rockslide threatened open pit. *Journal of Applied Geophysics*. 159, 304-311.
Kovanič, Ľ., Blišťan, P., Zelizňaková, V., Palková, J. (2017). Surveying of Open Pit Mine Using Low-Cost Aerial Photogrammetry. *In: Ivan, I., Singleton, A., Horák, J., Inspektor, T. (eds) The Rise of Big Spatial Data. Lecture Notes in Geoinformation and Cartography. Springer, Cham. https://doi.org/10.1007/978-3-319-45123-7_9.*
Kovanič, Ľ., Németh, Z. (2013). The application of geodetic methods for modelling the quarry walls and rock outcrops and their use in structural analysis: Case study from the quarry at Sedlice, Slovakia. *Mineralia Slovaca*, 45, 69 – 84.
Lopez-Pacheco, A. (2022). Ancient Japanese moats may lead to better open-pit mine designs. *CIM Magazine*, 30–31.
Martin, D., Stacey, P. (2018). Guidelines for open pit slope design in weak rocks. *CSIRO Publishing*.
Mello J., Elečko M., Pristaš J., Reichwalder P., Snopko L., Vass D., Vozárová A. (1996). Geologická mapa Slovenského krasu 1:50 000. Ministerstvo životného prostredia, Geologický služba Slovenskej republiky, Bratislava.
Narimani, S., Davarpanah, SM., Bar, N., Török, A., Vásárhelyi, B. (2023). Geological Strength Index Relationships with the Q-System and Q-Slope. *Sustainability.* 15, 11233. https://doi.org/10.3390/su151411233.
Nicholas, DE., Sims, DB. (2000). Collecting and Using Geologic Structure Data for Slope Design. In Hustrulid (ed.) *Slope Stability in Surface Mining, Society of Mining, Metallurgy, and Exploration*, Inc: Littleton.
Newman, J. (1890). Earthwork slips and subsidences upon public works: Their causes, prevention, and reparation. E. & F. N. Spon.
Pankow, KL., Moore, JR., Hale, JM., Koper, KD., Kubacki, T., Whidden, KM., McCarter, MK. (2013). Massive landslide at Utah copper mine generates wealth of geophysical data. *GSA Today*, 24(1).
Porathur, JL., S. Srikrishnan, S., Prasad Verma, Ch., Jhanwar, JC., Roy, P. (2013). Slope stability assessment
approach for multiple seams Highwall Mining extractions, *International Journal of Rock Mechanics & Mining Sciences* 70, 444–449.
Randolph, M. (2011). Current trends in mining. In P. Darling (Ed.), *SME mining engineering handbook* (3rd ed., pp. 11–19). Society for Mining Metallurgy and Exploration.
Read, J., Stacey, P. (2009). Guidelines for open pit slope design. *CSIRO Pub*., Collingwood.
Sdvyzhkova, O., Moldabayev, S., Babets, D., Bascetin, A., Asylkhanova, G., Nurmanova, A., Prykhodko, V. (2024). Numerical modelling of the pit wall stability while optimizing its boundaries to ensure the ore mining completeness. *Mining of Mineral Deposit*, 18(2), 1-10.
Snavely, N., Seitz, SM., Szeliski, R. (2008). Modeling the world from internet photo collections. *International Journal of Computer* Vision, 80, 189–210.
Špago, A., Jovanovski, M. (2019). Applicability of the Geological Strength Index (GSI) classification for carbonate rock mass Primjena "Geological Strength Index" (GSI) klasifikacije na karbonatne stijenske masive. *GEOTECHNICAL CHALLENGES IN KARSTISRM Specialised Conference/Međunarodna konferencija8. Savjetovanje Hrvatskog geotehničkog društvaOmiš – Split, Croatia, 11.-13.04.2019.ISBN 978-953-95486-8-9.*
Tsiambaos, G., Saroglou, ÆH. (2010). Excavatability assessment of rock masses using the Geological Strength Index (GSI). *Bull Eng Geol Environ*, 69, 13–27.
Utili S., Agosti A., Morales N., Valderrama C., Pell R., Albornoz G. (2022). *Mining Engineering* (extended abstracts), 45, 45–47.
Uysal, M., Toprak, AS., Polak, N. (2015). DEM generation with UAV photogrammetry and accuracy analysis in Sahitler hill. *Measurement* 73, 539–543.
Wijaya, AER., Karnawati, D., Srijono, Wilopo, W. (2013). Estimation of the geological strenght index system for cavity limestone layer in quarry area, Remang Central Java Province, Indonesia. *J. SE Asian Appl. Geol.*, 5(2), 71–77.